Solar Energy Materials & Solar Cells 96 (2012) 166–172

Contents lists available at SciVerse ScienceDirect

Solar Energy Materials & Solar Cells

journal homepage: www.elsevier.com/locate/solmat

Nano-indentation: A tool to investigate crack propagation related phase transitions in PV silicon

Prashant K. Kulshreshtha *, Khaled M. Youssef, George Rozgonyi

Department of Materials Science and Engineering, North Carolina State University, Raleigh, NC 27606-7907, USA

ARTICLE INFO

Article history:
Received 3 June 2011
Received in revised form
20 September 2011
Accepted 21 September 2011
Available online 4 October 2011

Keywords:
Nanoindentation
Solar
Silicon
Crack
Phase transformations
Amorphization

ABSTRACT

The initiation and propagation of a crack in a silicon wafer introduces local variations in the stress field and lattice structure through elastic energy release at crack-tip. In this study, the low load (<10 mN) capability of a Hysitron Triboindenter® has been employed to profile the exact distribution of stress and transformed Si-phases around micro-cracks in the PV silicon wafer. Hardness measurements showed an asymptotic drop, as the nanoindents were made closer to radial cracks or indent edges. Electron Back Scattered Diffraction (EBSD) and micro-Raman spectroscopic measurements, at the nano- and micro-scale, respectively, confirmed that the stress induced amorphization/phase change attributes to the hardness drop. Additionally, microscopic techniques including Atomic Force Microscopy (AFM) and Scanning Electron Microscopy (SEM) were applied to examine the nanoindent morphology impacted by local stress field and Si-phase change.

1. Introduction

A residual micro-crack in the wafer after sawing is the main source of breakage for the PV silicon substrates [1]. Micro-crack acts as a stress-raiser, which can lead to an unstable fracture, even at exceedingly small loads, particularly during handling and processing of thin PV wafers, currently about 150 μm [2–4]. Microscopic view of the wire-sawn wafer edges or surfaces exhibit sharp micro-cracks, scratches, and residual stress fields [1,5–7]. A selective etching of SiC grit induced surface damage cannot eliminate these sub-surface micro-cracks and associated plastic deformation [1,5,8]. We propose that a controlled Vickers indentation mimics the wire-saw induced surface damages, which has been applied to Si substrates to deliberately create brittle fracture induced cleavage (i.e. radial/median) and residual stress field related sub-surface (i.e. lateral) micro-cracks [9–11].

Radial or lateral micro-cracks form in silicon when plastic stresses increase beyond the fracture strength. Griffith's criterion stipulates that when released elastic energy, U, concentrated in the region of the crack tip overcomes the minimum energy, γ_s, associated with the appearance of a free surface, then a flaw or micro-crack becomes unstable and fracture occurs. Thus, according to Griffith's thermodynamic energy criterion for a given crack length, c, in a material with elastic modulus, E, the critical nominal fracture stress, σ_n, can be described as follows [12]:

$$dU/dc > [(\pi c/2E)(\sigma_n)^2] = 2\gamma_s \quad \text{thus,} \quad \sigma_n = \sqrt{(2\gamma_s E/\pi c)}. \tag{1}$$

However, fracture stress could be modified due to plastic flow, dislocation motion and stress relaxation in the vicinity of crack tip [13]. Using large-scale molecular-dynamics simulations, Buehler et al. [14] have shown that large deformations at the crack tip create an atomic-scale zone of hyperelasticity, which significantly affects the dynamics of brittle crack propagation. Unique crack instabilities in the form of the phase-transformations, crack-branching, and defect generations have been observed in the regions around the crack in the silicon [10,15–18]. For dynamically instable crack extension, the residual stresses at the crack-tip alter the elastic energy release rate in Si lattice ahead, depending on sign of stress [15].

Recently, due to competing cost pressures, PV Si substrate producers are employing new scenarios of faster than normal growth rates [19], larger size ingots/wafers (≈ 200 mm) [20,21], and thinner wafer sawing processes (<150 μm) [22]. Under enhanced thermal gradients, the point defects, impurities, and precipitates distribute inhomogeneously throughout the ingot. Our study of "ductile-like-fracture" in 200 mm diameter CZ wafers grown at faster rates revealed massive oxygen clustering and precipitation near the wafer to introduce sever warpage and local residual stresses greater than 100 MPa [23]. Several other researchers have studied the deformation around the micro-indent/cracks to determine the stress distribution using Raman micro-spectroscopy and TEM analyses [18,24–27]. However, the

* Corresponding author. Tel.: +1 919 760 5558.
E-mail addresses: prashant.kulshreshtha@gmail.com, pkkulshr@ncsu.edu (P.K. Kulshreshtha).

0927-0248/$ - see front matter © 2011 Elsevier B.V. All rights reserved.
doi:10.1016/j.solmat.2011.09.053

local material response to the applied load has not been examined for the distribution of stress and Si-phase in the proximity of a crack. Load-induced deformation of the Si lattice around the crack is the key to investigate the probability of crack propagation. It could provide a physical insight on the saw damage and consequential breakage of Si wafer above critical stresses. Thus, an estimate of the deformation volume and phase transformed region around the micro-crack, and its response to an applied load is critical to PV industry [1,28].

In this study, using nanoindentation technique, we have nanoscopically profiled the distribution of residual stress and associated phase transitions in the Czochralski (CZ) grown solar grade Si during a controlled micro-crack propagation. Careful examination of load (P) vs. displacements (h) curves determined the mechanical properties (i.e. hardness, modulus, etc.), phase changes and loading-induced deformation behavior of silicon. Additionally, measurements with Raman Spectroscopy and Electron Beam Scattered Diffraction (EBSD) were applied to quantify the residual stresses and confirm the phase transitions. AFM evaluation revealed the morphology and microstructure of nanoindents affected by stress relaxation processes.

2. Experimental details

Small samples of 10 mm × 5 mm were cleaved from the Czochralski (CZ) grown solar grade mono-crystalline silicon wafers (≈200 μm thick). Samples were single-side chemical–mechanical polished using colloidal silica solution and cleaned by acetone, methanol, and DI water. Vickers micro-indenter (Buehler Inc.) was used to create the micro-indents with alignment of indenter cleaved face along ⟨110⟩ direction, which resulted in radial micro-cracks emanating from indenter corners and few circularly extending lateral cracks from indenter edges. Low load (< 10 mN) nanoindentations were performed at the deformed region in the proximity of radial and lateral micro-cracks using a Hysitron TriboIndenter® with 50 nm radius Berkovich tip. The loading/unloading rate during the nanoindentation measurement was 100 μN/s. To establish a basic hardness data reference, atleast 5 nanoindents were made on pristine Si surface away from micro-indents. A Micro-Raman (Model: Horiba Jobin Yvon LabRam ARAMIS) tool with HeNe laser (633 nm) excitation was used to examine the phases at the pristine, micro-indented, and around micro-crack regions of silicon sample. HeNe Raman excitation of silicon surface through a 100× objective lens had penetration depth of ≈500 nm and resolution of about 2–3 μm. Later, EBSD measurements were performed near the nanoindents to capture the diffraction pattern corresponding to the amorphized silicon. Several arrays of nanoindents were also imaged using the Atomic Force Microscopy (AFM) unit available with the Triboindenter®. A Dimension 3000 AFM from Digital Instruments, Veeco (Fremont, CA) with Nanoscope©III software was used in the tapping mode to profile the imprint of the nanoindents at higher resolution.

3. Results and discussion

Fig. 1 shows the transmission infrared (IR) optical image superimposed with a schematic to represent a Vickers micro-indent on a monocrystalline Si sample with radial cracks at indent corners and lateral cracks at the edges. Sharp radial micro-cracks are formed due to rapid propagation of cleavage crack along energetically favorable direction ⟨110⟩ in Si [16,29]. Whereas, the lateral cracks at 45° from radial cracks, emanate from the base of plastic deformation zone during unloading and extending parallel to surface. The concentration of residual tensile stress

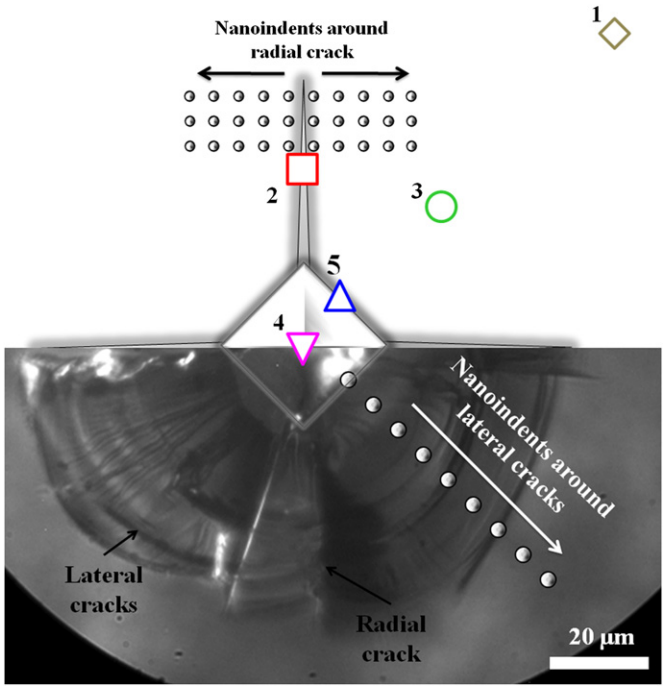

Fig. 1. Schematic of nanoindentation profiling and Raman spectroscopic measurements has been superimposed on an example infrared (IR) optical microscope image of a Vickers micro-indent created at 500 g load. The sharp radial cracks along cleavage faces and circularly extending subsurface lateral cracks due to plastic flow of Si around indent at 45° to the radial cracks can be observed in IR optical image. Using low load capability (< 10 mN), nanoindentation profiling has been performed around radial cracks or lateral cracks, as shown in the image by (●) and (○) dots along black and white arrows, respectively. The representative locations of Raman measurements in a quadrant have been shown, which correspond to: (1) pristine Si (undeformed lattice away from microindent), (2) radial cracks, (3) lateral cracks, (4) indent center and (5) indent edge.

field is the driving force for the lateral cracks, which at higher loads causes sub-surface damages and chip formation [10]. The darker contrast along lateral crack is the result of transmitted IR beam attenuation due to scattering from deformed lattice. The schematic in Fig. 1 represents locations of nanoindentation (spots along white and black arrows) and Raman measurements (marked as 1–5) around radial and lateral cracks to profile phase changes and quantify local stresses. In the following section, we estimate the distribution of stresses and Si phases using nanoindentation tests around brittle radial cracks in first sample.

3.1. Stress relaxation mechanism around "radial micro-cracks"

Fig. 2 shows a 3D AFM image ($8 \times 8\ \mu m^2$) representing only 4 of the 10 similar columns of atleast 4 nanoindents. Each indent was made using 1 mN load in the region of proximity to a radial micro-crack. Minimum separation between indents was atleast 1.5 μm to avoid interference between the nanoindent interaction volumes. The hardness data was extracted from load vs. displacement plot (i.e. P–h curves) of each nanoindent on both sides of the micro-crack. Fig. 2 shows the plot of average column hardness vs. distance of that particular column from the microcrack. The nanoindent columns farthest from the radial crack had average hardness of 10.1 ± 0.38 GPa (left) and 10.21 ± 0.51 GPa (right), which is comparable to the bulk hardness of the sample (10.59 ± 0.11 GPa). The hardness gradually dropped to 6.7 ± 0.73 GPa and 5.4 ± 1.37 GPa, respectively, on left and right sides of the crack, as nanoindent column were made closer to the crack. The nearest columns of nanoindents were only 0.5 μm away from the radial micro-crack. Fig. 3 represents the actual P–h